Evaluating the Application of PPP Techniques to ARAIM Using Flight Data

R. Eric Phelts, Kazuma Gunning, Juan Blanch, Todd Walter
Stanford University

ABSTRACT

Traditional ARAIM solution separation techniques assume measurement errors are uncorrelated from one epoch to the next. They bound errors with relatively large sigmas to compute provably-safe protection levels. PPP-based techniques assume measurement errors have a degree of time correlation. These approaches leverage filtering and estimation to calibrate errors and reduce measurement uncertainty over time. This paper uses flight data to assess the ability of PPP-based solution separation techniques to provide integrity for ARAIM users during flight. It compares time-filtered protection levels to those computed using traditional "snapshot" approach. It is shown that PPP with integrity is capable of producing significantly smaller protection levels that also show improved robustness to aircraft dynamics.

BACKGROUND

Solution Separation: Snapshot vs PPP

Advanced Receiver Autonomous Integrity Monitoring (ARAIM) is implemented using solution separation. Solution separation computations presume one or more GNSS satellites in may be faulted and iteratively compute multiple position solutions comprised of subsets of the satellites in view (N, N-1, N-2, etc.) to ensure that at least one of the solutions is fault-free. Using assumptions on the nominal and faulted uncertainty of the solutions, conservative horizonal and vertical protection levels (PLs) can be computed by bounding the uncertainty from all the solutions. This assures (to a targeted level of probability) that the user position is contained within these limits. [1]

Traditional solution separation techniques generally operate as a "snapshot". The basic measurements are dual-frequency, carrier-smoothed code, and errors are generally assumed to be uncorrelated from epoch-to-epoch. This requires that errors at each time step are conservatively bounded with large sigmas designed to protect the user against the worst-case error. These assumptions minimize the complexity and computational cost of the solution by providing a robust, provably-safe bound. However, the protection levels computed are relatively large. In addition, they can change suddenly from one epoch to the next due to changes in available satellites or platform dynamics. This can make meeting performance goals (e.g., continuity) for aircraft approaches more challenging.

Solution separation using PPP-based techniques implement an extended Kalman filter (EKF) to filter measurements over time. The basic measurements are dual-frequency code and carrier, and errors are assumed to have some correlation from each time step to the next. Accordingly, these techniques leverage higher-quality measurements (i.e., carrier-based as opposed to code-based) to smooth and reduce large sigmas and to estimate (and calibrate) errors over time. The complexity associated with defining and characterizing the decorrelation models for the errors (i.e., so that the nominal covariance produced by the EKF conservatively describes the actual error) is significant [2][3]. Also, the computational cost of estimating the error states may be substantially higher than with traditional snapshot approach. However, the computed protection levels provide integrity and are often significantly smaller [3]. In addition, the filtering makes them more robust to platform dynamics, which makes them well-suited for aircraft in flight.

Flight Data: Outages and Cycle Slips

ARAIM performance may be significantly affected by aircraft dynamics [4]. Specifically, banking can induce satellite outages and cycle slips. Outages weaken the constellation geometry and can cause sudden changes in the protection level. Frequent cycle slips prevent code measurements from being smoothed, potentially inflating protection levels of carrier-smoothed code measurements for extended periods of time.

When the outages and cycle slips are computed as a rate, a trend can be seen. Both increase notably as the relative elevation to the satellites decrease. Figure 1 plots outages as a function of the apparent elevation of the satellites (relative to the aircraft). Cycle slips on GPS L1-L5 and Galileo El-E5a are plotted in Figures 2. (More details on the outage and cycle analysis can be found in [4].)

This paper uses the flight data used to generate data from [4] used to generate Figures 1 and 2. It shows that significant advantages of PPP can be retained even during aircraft maneuvers, when outages and cycle slips threaten ARAIM continuity and availability most.

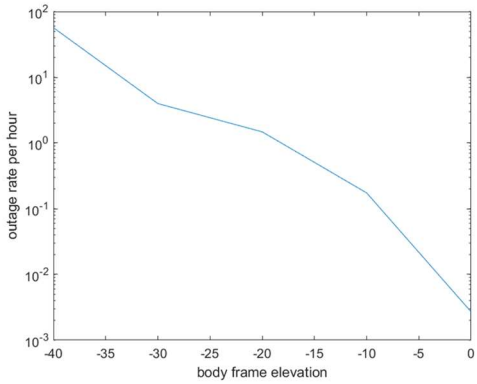

Figure 1. Outages as function of body frame or "apparent" elevation angle during aircraft banking.

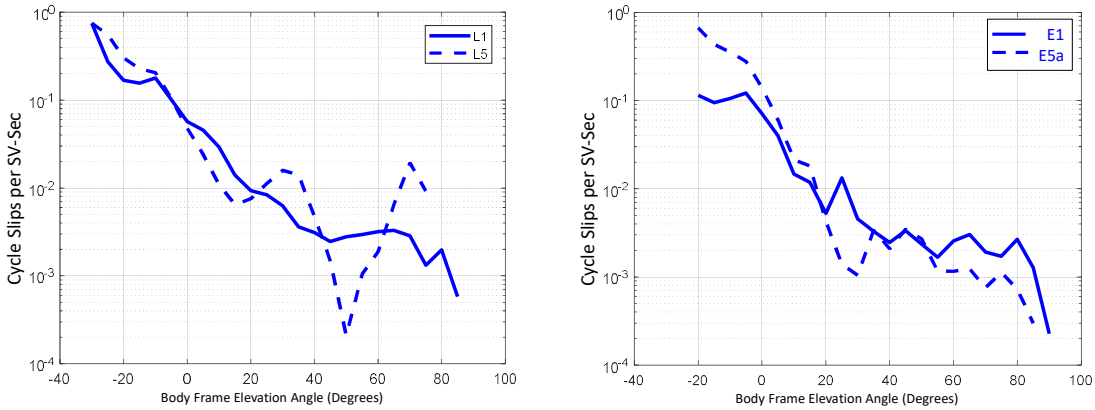

Figure 2. Cycle slip rate (per satellite-second) for GPS L1-L5 and E1-E5a

MODEL ASSUMPTIONS

Traditional "snapshot" solution separation approach is well-established and was implemented according to the standards outlined in [1]. For this paper, the constellations were limited to GPS and Galileo and the prior probabilities assumed for satellite and constellation faults were as follows: $P_{sat} = 10^{-5}$, $P_{const,GPS} = 10^{-8}$ and $P_{const,GAL\text{-}e\text{-}4} = 10^{-4}$.

The PPP algorithm with solution separation is implemented using an extended Kalman filter (EKF) using dual frequency code and carrier phase measurements (from GPS and Galileo) with estimated parameters comprising the receiver position, clock biases for each constellation in use, a tropospheric delay, float ambiguities for each tracked carrier phase, and multipath contributions. Many of the details of the implementation can be found in [2].

The predicted dual frequency code and carrier phase measurements can be modeled as follows:

Dual frequency carrier phase:

$$\Phi_{if}^{(i)} = \left\|x_s^{(i)} - \hat{x}_{rx}\right\| + c\left(\hat{b}_{rx,c} - b_s^{(i)}\right) + m^{(i)}\widehat{\Delta T}^{(i)} + b_{pwu}^{(i)} - \hat{A}^{(i)} + \mathrm{R_m} + \hat{M}^{(i)} + \hat{\epsilon}_{brdc}^{(i)} + \epsilon^{(i)} \quad (1)$$

Dual frequency code phase:

$$\rho_{if}^{(i)} = \left\|x_s^{(i)} - \hat{x}_{rx}\right\| + c\left(\hat{b}_{rx,c} - b_s^{(i)}\right) + m^{(i)}\widehat{\Delta T}^{(i)} - \widehat{DCB}_{rx}^{(i)} + \mathrm{R_m} + \hat{M}^{(i)} + \hat{\epsilon}_{brdc}^{(i)} + \epsilon^{(i)} \quad (2)$$

Where

$x_s^{(i)}$- satellite position provided by external precise orbit product

$\hat{x}_{rx}$- estimated receiver position

$\hat{b}_{rx,c}$- estimated receiver clock bias

$b_s^{(i)}$- satellite clock offset provided by external precise orbit product

$m^{(i)}$- tropospheric mapping function

$\widehat{\Delta T}^{(i)}$- estimated delta tropospheric delay

$b_{pwu}^{(i)}$- carrier phase wind-up

$\hat{A}^{(i)}$- estimated float carrier phase ambiguity

$\hat{M}^{(i)}$- estimated multipath delay on the signal

$\widehat{DCB}_{rx}^{(i)}$- estimated receiver differential code bias per signal (shared across SVs)

$\mathrm{I}^{(i)}$- ionospheric delay/advance

$\mathrm{R_m}$- Other modeled effects. This includes relativistic effects, solid earth tide modeling, satellite antenna phase center offset and variation, ocean loading, modeled tropospheric delay, and any other desired range models. These are strictly modeled and not estimated.

$\hat{\epsilon}_{brdc}^{(i)}$- error due to broadcast navigation message orbit and clock

$\epsilon^{(i)}$- other unaccounted for errors

The estimated states are indicated by a carrot over the symbols. Here, the estimated states include the position, velocity, receiver clock biases, tropospheric delay, carrier phase ambiguities, multipath error, receiver differential code bias, and broadcast orbit and clock error.

PPP techniques typically utilize precise ephemeris information obtained from a global network of ground reference stations [2]. Snapshot solution separation techniques, however use only ephemeris information broadcast from the satellites. For a proper comparison of the protection levels computed by the each, the PPP filter was constrained to use this broadcast information.

The model applied here is mostly typical of a traditional PPP implementation with one significant exception—the state tracking the error contribution of the broadcast orbit and clock on each line of sight. The error contributed by the broadcast orbit and clock is handled by the filter leveraging a characterization of the rate of change of the error then including it as an estimation state for each line of sight and only adding enough process noise to capture the slowly changing error. A characterization of the rate of change of the error in the broadcast orbit and clock and process noise (for GPS) is given in [3]. Complete tables of initial state uncertainties and additional settings for process and measurement noise are provided in [2].

RESULTS

Flight data collected over a period of approximately one year was used to evaluate ARAIM performance through momentary outages and cycle slips and due to aircraft dynamics. A multi-constellation, multi-frequency receiver (Trimble BX935-INS) tracked GPS, (L1 C/A and L5) and Galileo (E1 and E5a). This receiver is installed in a Global 5000 jet owned and operated by the William J. Hughes FAA Technical Center. It records and stores GNSS measurements whenever flights are taken. [5] The data collection effort of this paper included data recorded over approximately 35 flights from September 2017 to April 2018.

Figure 3 shows the trajectory and altitude information corresponding to a single flight (Flight #6) taken on September 20, 2017. Figure 4 compares the corresponding horizontal and vertical protection levels computed using snapshot and "broadcast" PPP techniques. (For an additional reference, protection levels computed using precise PPP (i.e., with corrections) are also plotted. [2])

Several things are readily apparent from these comparisons. First, after the initial time required for convergence, there is a substantial reduction in the PLs using the broadcast PPP-based approach. (The precise PPP PLs, as expected, produce the largest reduction but use additional information not available to the snapshot method.) In addition, the snapshot solution separation PLs vary significantly due to cycle slips and momentary satellite outages. Figure 5 shows the number of satellites tracked by the receiver during this flight; red circles plotted on the snapshot protection level line indicate where satellites are coming into and out of view. Despite numerous abrupt changes in number of measurements and measurement quality, the EKF of the PPP techniques produces PLs that are relatively smooth and continuous.

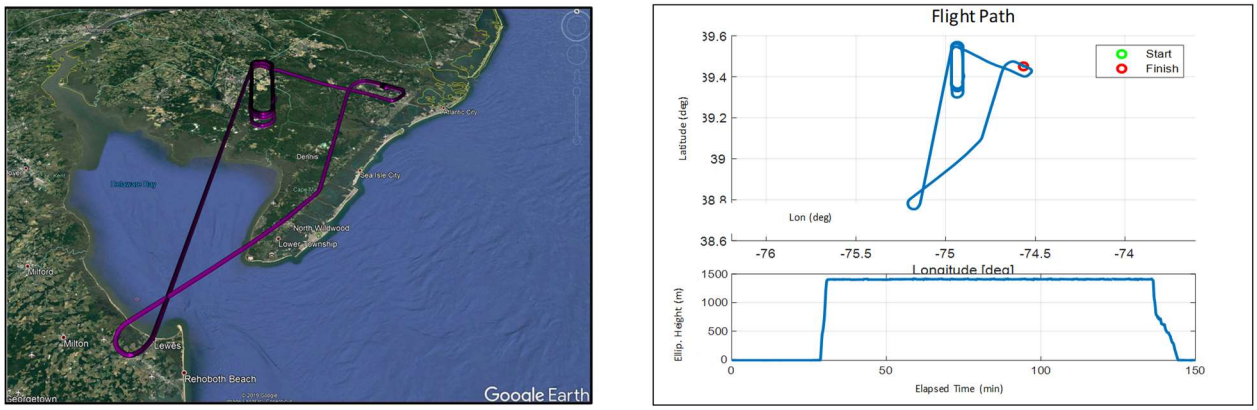

Figure 3. Flight path and altitude information for flight #6 (September 20, 2017).

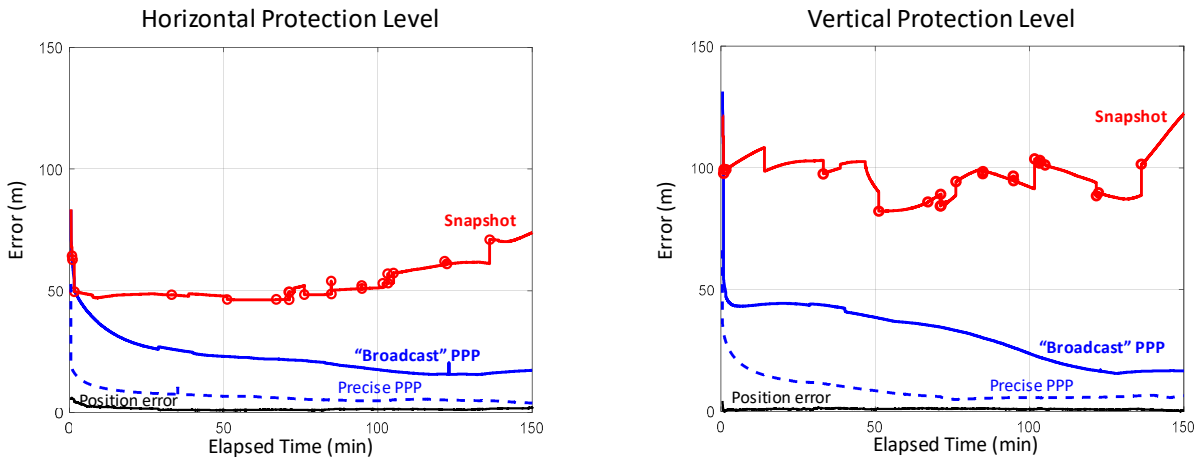

Figures 4. Horizontal (left) and Vertical (right) Protection Levels for Flight #6 (September 20, 2017). (Red circles indicate a satellite being dropped or re-entering the solution.)

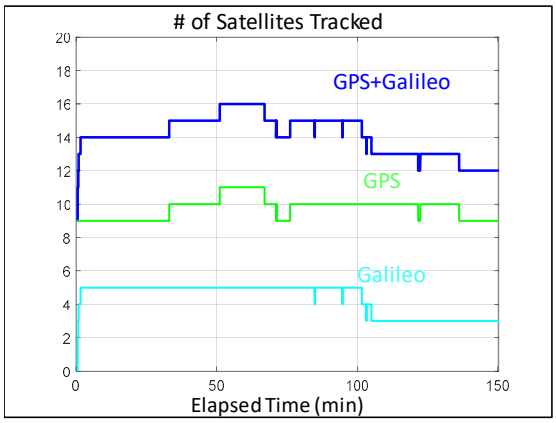

Figure 5. Number of satellites tracked for Flight # 6 (September 20, 2017).

Figure 6 shows the trajectory and altitude information corresponding to Flight #4 taken on September 15, 2017. Figures 7 compares the horizontal and vertical PLs for snapshot solution separation and the PPP-based techniques.

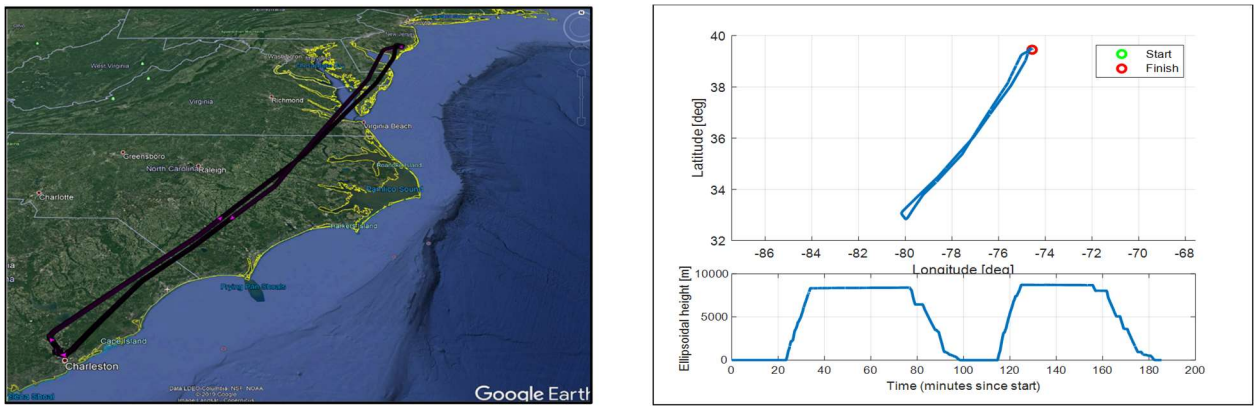

Figure 6. Flight path and altitude information for flight #4 (September 20, 2017).

As was in the case of Figure 4, the PLs in Figure 8 reveal that a substantial reduction in the mean PLs computed using the PPP-based approach. And the snapshot solution-separation approach displays even more variations due to

momentary satellite outages. Some of the cycle slips affected enough satellites to introduce brief spikes in the PPP solution as well. These re-converge quickly, but they suggest that some tuning of the EKF can still be done to mitigate these interruptions. Still, the filtered approach produces PLs that are more robust to the outages and are substantially smaller than with the snapshot method.

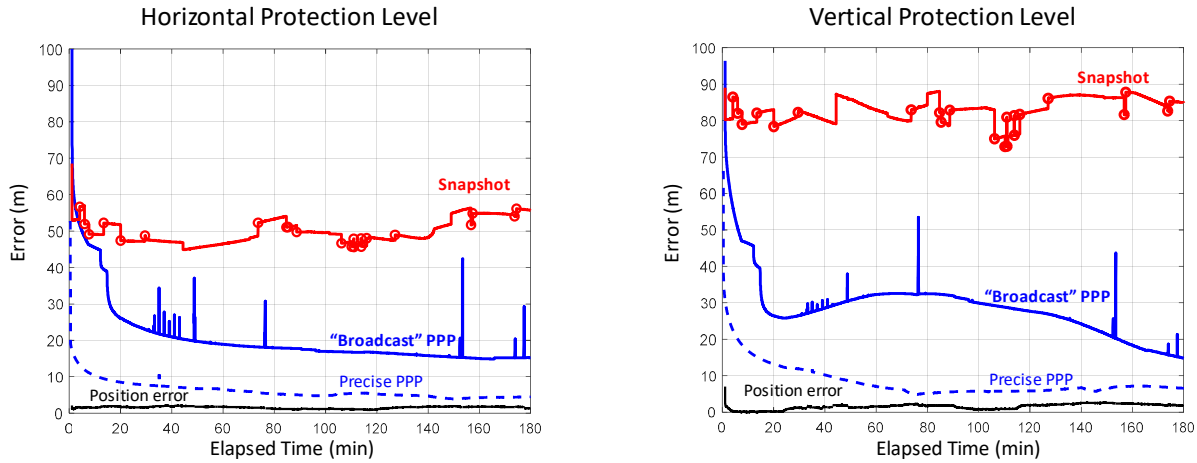

Figures 7. Horizontal (left) and Vertical (right) Protection Levels for flight #4 (September 15, 2017). (Red circles indicate a satellite being dropped or re-entering the solution.)

Figures 8 compares the horizontal and vertical PLs computed using snapshot solution separation and PPP techniques for Flight #20—where the airplane remained stationary on the runway. In the absence of flight dynamics, the levels for all the approaches were relatively smooth. However, a few discontinuities can still be observed for the snapshot case. Also note, in the case of the broadcast PPP, the convergence time is noticeably longer. This is likely because the integer ambiguity resolution in the solution took longer to converge without platform motion.

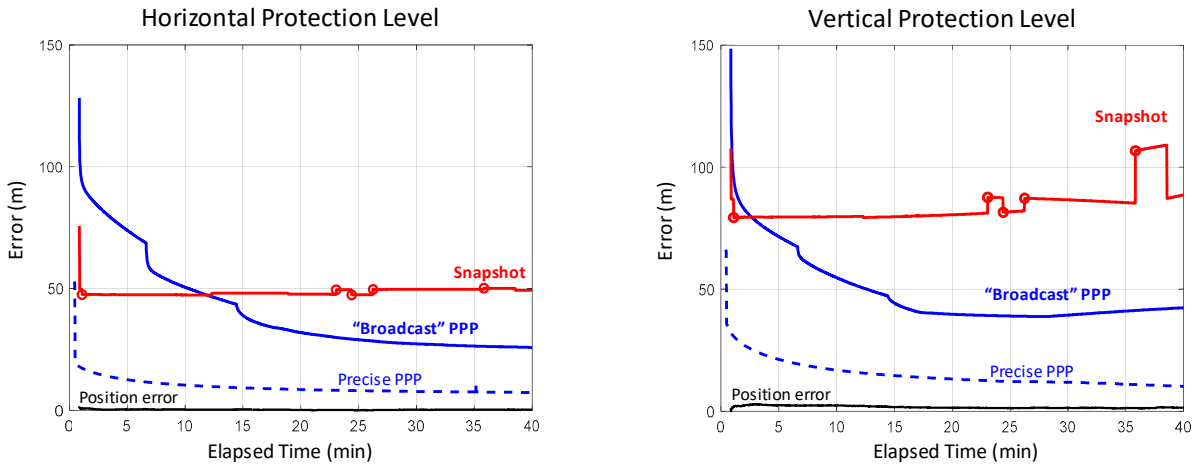

Figures 8. Horizontal (left) and Vertical (right) Protection Levels for a stationary aircraft (Flight #20, December 4, 2017). (Red circles indicate a satellite being dropped or re-entering the solution.)

The mean HPLs and VPLs for both techniques are summarized in Figure 9. The PPP approach consistently produces protection levels anywhere from 30 to 75% smaller than those computed using the snapshot approach. The mean PLs for the PPP techniques were always below those computed with the snapshot method.

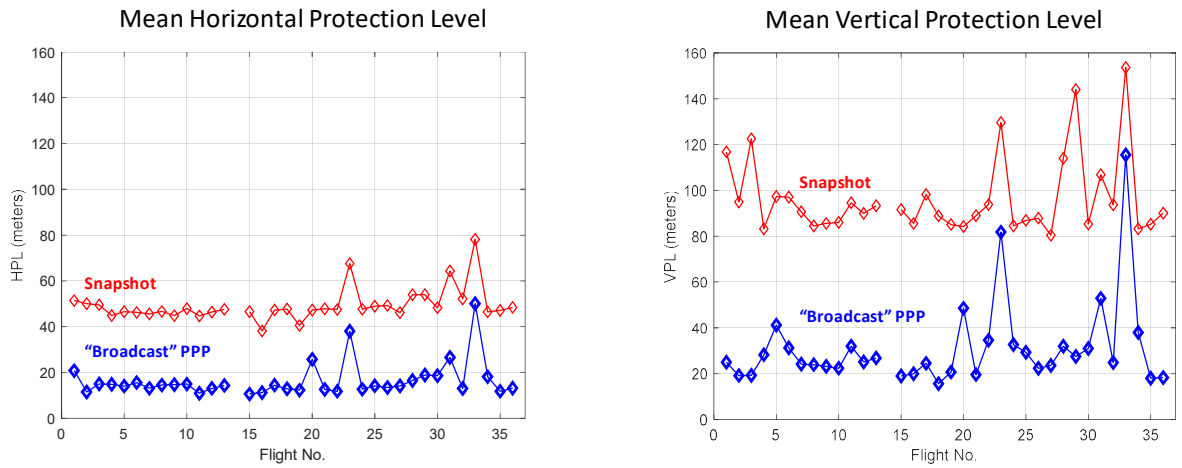

Figure 9. Comparison of mean horizontal and vertical PLs for "snapshot" vs a PPP-based technique.

CONCLUSIONS

Data from 35 flights was used to compare ARAIM protection levels computed by traditional "snapshot" solution separation vs a PPP-based approach during both in-flight and several static scenarios. It was observed that the filtering of PPP methods yields mean PLs approximately 30% to 75% of those computed using traditional methods in all cases. This improvement can be attributed to exploiting—through filtering and estimation—carrier phase-based measurements and a time-correlation of the errors. In addition, the EKF employed by PPP approach demonstrated improved robustness to outages and cycle slips induced by aircraft dynamics. Despite the increased complexity and computational cost, it is believed that PPP approaches hold promise for significantly improving ARAIM performance.

REFERENCES

[1] Working Group C, ARAIM Technical Subgroup, Milestone 3 Report, February 26, 2016. Available at: http://www.gps.gov/policy/cooperation/europe/2016/working-group-c/ http://ec.europa.eu/growth/tools-databases/newsroom/cf/itemdetail.cfm?item_id=8690

[2] Gunning, Kazuma, Blanch, Juan, Walter, Todd, de Groot, Lance, Norman, Laura, "Design and Evaluation of Integrity Algorithms for PPP in Kinematic Applications," *Proceedings of the 31st International Technical Meeting of the Satellite Division of The Institute of Navigation (ION GNSS+ 2018)*, Miami, Florida, September 2018, pp. 1910-1939.

[3] Gunning, Kazuma, Blanch, Juan, Walter, Todd, "SBAS Corrections for PPP Integrity with Solution Separation," *Proceedings of the 2019 International Technical Meeting of The Institute of Navigation*, Reston, Virginia, January 2019, pp. 707-719.

[4] Phelts, R. Eric, Blanch, Juan, Gunning, Kazuma, Walter, Todd, Enge, Per, "Effect of Aircraft Banking on ARAIM Performance," *Proceedings of the 31st International Technical Meeting of the Satellite Division of The Institute of Navigation (ION GNSS+ 2018)*, Miami, Florida, September 2018, pp. 2632-2641.

[5] Phelts, R. Eric, Blanch, Juan, Chen, Yu-Hsuan, Enge, Per, Riley, Stuart, "ARAIM in Flight Using GPS and GLONASS: Initial Results from a Real-time Implementation," *Proceedings of the 29th International Technical Meeting of The Satellite Division of the Institute of Navigation (ION GNSS+ 2016)*, Portland, Oregon, September 2016, pp. 3264-3269.